Thin films of $PtAl_2$ and $AuAl_2$ by solid-state reactive synthesis

S. Supansomboon[1], A. Dowd[1], A. Gentle[1], E. van der Lingen[2], and M.B. Cortie[1*]

[1]*Institute for Nanoscale Technology, University of Technology Sydney*

PO Box 123, Broadway, NSW 2007, Australia

[2]*Department of Engineering and Technology Management, University of Pretoria*

Lynnwood Road, Hatfield, Pretoria, South Africa

Abstract

The intermetallic compounds $AuAl_2$ and $PtAl_2$ are colored purple and yellow respectively. In the past they have been prepared by bulk melting techniques or by co-deposition in a magnetron sputterer. Here, however, we investigate films of $AuAl_2$, $PtAl_2$ and $(Au,Pt)Al_2$ prepared by *sequential* physical vapor deposition of the elements, followed by *in situ* solid-state reaction. The microstructure, dielectric functions, optical properties and thermal stability of the resulting films are characterized and compared to those prepared by bulk melting or co-deposition. The $(Au,Pt)Al_2$ films show a color gamut that stretches from purple to brassy yellow depending on composition and microstructure. High temperature synchrotron X-ray diffraction experiments show that the $(Au,Pt)Al_2$ phase is metastable, decomposing when heated above 420 °C. In contrast, the pure $AuAl_2$ or $PtAl_2$ phases are stable to about 580 °C before they oxidize or decompose. The alternative possibility of producing the purple-to-yellow color gamut by depositing optical stacks of very thin films of $AuAl_2$ and $PtAl_2$ is also assessed. Either scheme will provide a range of colors lying between those of the binary compound endpoints. Calculations predict that deposition of $AuAl_2$ onto $PtAl_2$ will produce more intense colors than vice versa, an unexpected finding that is worth further investigation.

Keywords: intermetallic compounds, $PtAl_2$, $AuAl_2$, color, optical properties, solid state synthesis

[*] Corresponding author: Tel.: +61 295142208; *E-mail address*: michael.cortie@uts.edu.au (Michael Cortie).

1. Introduction

Metallic elements have a rather limited range of intrinsic colors, with most being silver- or gray-colored. Copper and gold stand out as rare exceptions due to their respective red-orange and yellow hues. More metallic color options are available, however, when alloys and intermetallic compounds are considered. For example, the 'yellow', 'white', 'red', 'pink' and 'green' colors of commercial gold alloys are obtained by substituting elements such as silver, copper, palladium and zinc for part of the gold. Some intermetallic compounds, particularly those with the B2 (cP2) and C1 (cF12) structures, also have interesting and attractive metallic colors [1]. For example, the C1-structured compounds $PtAl_2$ and $AuAl_2$ (which have anti-fluorite structures based on a geometric inversion of the structure of the compound CaF_2[2]) are brassy yellow and metallic purple respectively. Both are known for producing eye-catching effects in specialized jewelry [3-7] and they have been the subject of a comprehensive recent investigation by Furrer and Spolenak [8]. The relatively unusual dielectric functions of $PtAl_2$ and $AuAl_2$ have also been previously investigated [4, 9-15] and their possible application in spectrally-selective filters or plasmonic devices discussed [4, 9, 10].

Since $AuAl_2$ and $PtAl_2$ share the same crystal structure the question arises of whether or not they can form a single $Au_xPt_{1-x}Al_2$ ($0<x<1$) phase field that spans the ternary phase diagram [8]. Furthermore, if such a ternary intermetallic phase exists, then there is the issue of whether it is metastable relative to decomposition to the binary end members. We could not resolve this question by a CALPHAD calculation because the commercially thermodynamic databases available to us did not have sufficient data yet for the calculation of this ternary system (due primarily to a lack of data for Al-Pt). On the other hand, Furrer and Spolenak [8] found experimental evidence for a continuous $(Au,Pt)Al_2$ solid solution, and its existence was also assumed in a recent Density Functional Theory study [10]. In contrast, microstructural evidence from other C1 systems suggests an equilibrium state of mutual immiscibility for compounds of this type. For example, the

compounds $AuIn_2$ and $PtIn_2$ [5] and $AuAl_2$, $AuIn_2$ and $AuGa_2$ [6] are reported to be mutually insoluble.

It has been shown that materials with a C1 structure and a stoichiometry of the form $Au_xPt_{1-x}Al_2$ ($0<x<1$) will have a color that shifts from purple to brassy yellow, via a peach-colored intermediate, as x varies for 1 to 0 [8, 10]. Of course, such a gradation of color does not only occur in a solid solution series and would also be expected in duplex microstructures of $AuAl_2$ and $PtAl_2$. Indeed, colors of intermediate nature are reported for duplex mixtures of $AuAl_2$, $AuGa_2$, $AuIn_2$ and $PtIn_2$ [5, 6]. Whatever the origin, the range of colors, and the fact that these materials have a high precious metal content, make them of interest to the jewelry industry.

The challenge, however, is to find convenient ways to fabricate these materials because intermetallic compounds are notoriously brittle. For bulk samples the processing options that have been investigated include traditional casting [5, 6], powder metallurgy [16, 17] and vacuum-arc melting [18]. For thin films physical vapor deposition (PVD) is an obvious choice. Furrer and Spolenak [8] successfully produced thin films with C1 structure using the *simultaneous* co-deposition of Al, Pt and Au but it is challenging to precisely control the sputtering rates of three targets simultaneously in an industrial context. Therefore, we investigated whether suitable coatings could be produced by deposition of one or two elements at a time followed by an annealing heat treatment to drive the solid-state reaction $M+2Al \rightarrow MAl_2$. To do this we used PVD to produce a range of single-layer, bi-layer and multi-layer nanoscale films comprised of Au, Pt and Al. Our overall objectives were to determine how the desired intermetallic compounds might be synthesized, whether a $Au_xPt_{1-x}Al_2$ solid solution can form or not (and if so whether it is thermally stable), the extent to which the microstructure of coating of these materials controls their color, and whether the deposition of nanoscale optical stacks of $AuAl_2$ alternated with $PtAl_2$ might provide an alternative means to control the color. We also fabricated and characterized a range of bulk samples for comparison purposes.

2. Material and methods

Thin film samples were prepared by direct current, magnetron sputtering and bulk samples by vacuum arc melting. For the thin film samples, sputtering targets of Au, Pt and Al, each with a purity of at least 99.99%, were used and set 150 mm away from the rotating substrate. The base pressure in the chamber was less than $1x10^{-4}$ Pa (10^{-6} Torr). During the deposition, Ar gas flowed at a pressure of 0.3 Pa (2.0 mTorr), with a flow rate ranging from 15-90 sccm. Various substrates were used, depending on the requirements for further characterization. For optical characterization, the thin films were deposited onto glass slides that had been cleaned with a detergent solution in a sonicator for 20 minutes, then rinsed with distilled water and dried under N_2. For laboratory X-ray diffraction at room temperature films were deposited onto silicon wafers while, for high-temperature synchrotron X-ray diffraction, tantalum or austenitic stainless steel foils were used as substrates. The various non-glass substrates were cleaned with acetone in a sonicator, then rinsed with ethanol and dried under N_2. Bulk samples of $AuAl_2$, $(Au_{0.5}Pt_{0.5})Al_2$, $(Au_{0.7}Pt_{0.3})Al_2$, $(Au_{0.9}Pt_{0.1})Al_2$ and $PtAl_2$ were produced from the elements by vacuum arc melting on a water-cooled copper hearth. This technique is associated with a rapid cooling rate from the molten state but nevertheless provides a well crystallized sample, Fig. 1(a).

Various designs of the films were investigated, including stacks of the pure elements or stacks of binary mixtures. A quartz crystal monitor and controller were used for measuring and controlling deposition rate and thickness of each element. The composition of compounds was controlled by setting the appropriate amperage and wattage levels. Some examples of thin films of the intermetallic compounds in stacks in different sequences are shown in Fig. 1(b). Films were either deposited onto substrates held at 400°C or deposited at room temperature and annealed thereafter at 400 °C in a tube furnace under N_2 flow.

As a preliminary investigation these samples were analyzed for their composition and morphology using a Zeiss Supra 55VP scanning electron microscope (SEM) with Oxford energy

dispersive spectrometry (EDS) and a Zeiss Evo LS15 SEM with a Bruker EDS Quantax400. The Zeiss Supra 55VP is a field emission SEM (FESEM) and was operated in a high vacuum mode. An acceleration voltage of 5-20 kV was applied and imaging was usually in the 'in-lens' and 'backscattered' modes. The Zeiss Evo LS15 is a thermionic tungsten electron gun SEM and was employed when just an elemental analysis was needed. Samples were examined along a normal to their plane, or side-on after fracture of the substrate.

More precise information of internal structure was obtained by examination of cross-sections with a JEOL 2200FS high resolution transmission electron microscope (TEM). This has a field emission gun and was operated at 200 kV. A cross-sectional area of selected thin film specimens was prepared by using the sandwich technique and tripod polishing, followed by precision ion polishing system (PIPS). Bright field (BF) and dark field (DF) images were obtained, as well as electron diffraction patterns. EDS analyses were performed in line scan and area mapping through the cross-sectional area.

X-ray diffraction (XRD) was conducted using a Siemens D5000 X-ray diffractometer or at the powder diffraction beamline at the Australian Synchrotron. In both instances the samples were set up in grazing incidence mode. In the case of the laboratory XRD, Cu $K\alpha_1$ radiation ($\lambda = 1.54056$ Å) was used, the angle of incidence was 0.5°, 2θ was scanned between 20° and 90° and counts were accumulated for 3 seconds at each step. In the case of the synchrotron measurements the substrate was a metal foil, as previously mentioned. The samples were placed on the platinum heating element of an Anton Paar furnace under argon (Ta substrate) or vacuum (stainless steel substrate) and measurements taken while the temperature was raised. A wavelength of 0.06199 nm was used for the experiments on Ta foil and a wavelength of 0.11261 nm was used for the experiments on the stainless steel substrates. Wavelengths were verified by calibration using NIST LaB_6 standard 660b. A slit height of 0.2 mm was used.

To determine the optical properties, the reflectance and transmittance of samples were measured with a Perkin-Elmer Lambda 950 UV/Vis spectrophotometer. The WVASE32 program of J A Woollam was applied to model and calculate the dielectric functions (*n* and *k*) from measured reflectance and, where available, transmittance data. The dielectric functions of the co-sputtered samples were also extracted from data obtained with a J A Woollam variable angle spectroscopic ellipsometer (VASE). The program OpenFilters [19] was used to model the performance of multilayer thin films, based on the newly measured dielectric functions. The dielectric functions obtained from measurements were also used for simulating color in the *L*a*b** color space defined by the CIE system [20].

3. Results

3.1 Formation of single-layer thin films

Thin films of $AuAl_2$ or $PtAl_2$ could be fabricated by depositing Al as the first layer, followed by an appropriate amount of Au or Pt (the configuration of Fig. 1(b)(i)). Interdiffusion of the elements and formation of the intermetallic compound could be achieved by annealing the bi-layer structure at 400 °C for 1 hour with care taken to avoid oxidation. X-ray diffraction shows that $AuAl_2$ or $PtAl_2$ was formed provided that close to the correct stoichiometry was laid down during deposition. These samples were silvery in the as-deposited state and only acquired the color of the C1 phase or phases after annealing. Color was affected by deviations from stoichiometry. Samples with a slight excess of Al (for example 72 at.%) had a pale purple color and a microstructure consisting of $AuAl_2$ and some interdendritic Al. Samples with the correct stoichiometry consisted of $AuAl_2$ and had the desired bright purple color. Decrease of the Al content to 60 at.% led to the precipitation of AuAl phase and a dramatic decrease in reflectance intensity and color saturation.

The lattice parameter of the $AuAl_2$ film and its bulk comparator sample were obtained by

Rietveld refinement and found to be 0.5993 and 0.5999 nm respectively, at room temperature. These values are in agreement with the 0.5995 to 0.5999 nm recorded for this compound in Pearson's Handbook [21] and the Joint Committee on Powder Diffraction Standards (JCPDS) cards number 00-017-0877 and 03-065-2984. The lattice parameters of the $PtAl_2$ film and bulk samples were found to be 0.5941 and 0.5923 nm respectively. Once again, these values are close to the published values of 0.5920 to 0.5930 nm, for example JCPDF cards number 00-003-1006 and 03-065-2983.

3.2 Co-deposition of Au and Pt onto Al

In order to investigate whether $PtAl_2$ and $AuAl_2$ could be mutually soluble, a series of samples were prepared in which Al was deposited as a first layer followed by the co-deposition of a mixture of Au and Pt as a second layer (the configuration shown in Fig. 1(b)(ii)). These are designated here as Al/(Au,Pt)). The reverse arrangement, in which a mixture of Au and Pt was first deposited followed by Al (designated here as (Au,Pt)/Al) was also investigated. Both types of sample were silvery in the as-deposited state and only acquired the color of the C1 phase or phases after annealing at 400°C for 30 minutes

XRD of the co-deposited Au and Pt layers produced in the present work indicated that they were in the form of a metastable fcc solid solution, Fig. 2(a), with a lattice parameter of 0.4006 nm. This obviously lies between that of pure Au films (0.4077 nm for films in the present work, compared to a literature value of 0.4079 nm for the bulk element) and pure Pt films (0.3935 nm for our Pt films, compared to a literature value of 0.3924 nm for the bulk element). The top layer of the sample of Fig. 2(a) was 53.3 at% Au and 46.7 at.% Pt so, from Vegard's rule, a lattice parameter of 0.4006 nm would be expected for a solid solution, in excellent agreement with the observed value. The XRD data unequivocally show that co-deposited Au and Pt are in a metastable solid solution rather than the mixture of separate Au and Pt phases expected from thermodynamic equilibrium.

The most consistent formation of the desired intermetallic compounds was from samples in which the Al was protected from oxidation by a top layer of noble metal. After heat treatment, an Al/(Au,Pt) sample (20 nm of Au plus Pt) yielded an X-ray pattern matching the C1 structure, Fig. 2(b). EDS analysis of the sample of Fig. 2(b) indicated that its composition was 65 at.% Al, 23 at.% Pt and 12 at.% Au. Rietveld analysis of this sample yielded a lattice parameter of a=0.5952 nm, which is close to a value of 0.5958 nm that could be expected from applying Vegard's Law to a mixture of $AuAl_2$ and $PtAl_2$ in the composition ratio of the film.

The results of TEM-EDS analysis and high resolution cross-sectional images of the Al/(Au,Pt) film are shown in Fig.3. The most prominent lattice fringes have a spacing of ~0.30 nm and match the (002) plane of $AuAl_2$ or $PtAl_2$. In contrast, the pure elements Al, Pt or Au do not have any lattice fringes with a spacing greater the ~0.23 nm of their (111) planes. Chemical analysis shows that coating is made of two layers, an upper layer containing a mixture of Pt, Au and Al, and a bottom layer of Al plus Si. There is a slight decrease in the Pt:Au ratio from top to bottom in the upper layer. It is clear that the annealing heat treatment had caused a polycrystalline solid solution of the $(Au,Pt)Al_2$ type to form by reaction of the top layer with the upper part of the Al bottom layer, while Si from the substrate had diffused into the remainder of the lower part of Al bottom layer. The bottom part of sample was amorphous in electron diffraction and is evidently oxidized.

An Al/(Au,Pt) sample consisting of ~200 nm of Al followed by a co-deposition of a combined ~100 nm of Au and Pt (Pt 46 at.%, Au 54 at.%) was subjected to XRD in a synchrotron beamline while being heated. Only the peaks due to the elements Pt and Al (and those of the stainless steel foil substrate used) are evident up to a temperature of 310 °C. (The lattice parameter of Au is similar to that of Al and was masked by the peak of the relatively thick Al underlayer). At 312 °C the peaks of a C1 phase appear with a lattice parameter of 0.599 nm. The variation of the observed lattice parameter of this C1 phase with temperature is plotted in Fig. 4. The results of both full pattern Rietveld refinement and single peak analysis are shown and are very similar. Also

shown in Fig. 4 is the estimated trend line for the high temperature lattice parameters of $AuAl_2$ and $PtAl_2$ (obtained by extrapolating from room temperature using an estimate of $13x10^{-6}$ K^{-1} for the coefficient of thermal expansion). It is clear in Fig. 4 that the C1 phase formed has a lattice parameter intermediate between that of $AuAl_2$ and $PtAl_2$. Indeed, as before, its value is very close to what might have been expected by applying Vegard's rule to a mixed solid solution of $(Au,Pt)Al_2$. However, raising the temperature above ~350 °C led to the appearance of Pt_2Al_3 phase, Fig. 5, a process accompanied by a decrease in the amount of MAl_2 phase. There is a concomitant increase in the lattice parameter of the C1 phase remaining to the value expected for $AuAl_2$. Clearly, the Pt content of the original $(Au,Pt)Al_2$ phase has transferred to the newly formed Pt_2Al_3 phase, leaving the remaining $(Au,Pt)Al_2$ richer in Au. Peaks for a further phase, possibly AuAl, appear at about 380°C, and are the result of the Au-rich C1 phase decomposing further. All C1 phase is consumed by 430°C. The diffraction pattern becomes even more complex above 500°C with evidence appearing for Au_4Al and PtAl. Evidently, some of the Al is being consumed by oxidation, notwithstanding the protective sample environment, and the remaining metallic material is becoming enriched in the noble metals. The sequence of reactions as this sample approaches equilibrium is therefore:

$(Au,Pt)+Al \rightarrow (Au,Pt)Al_2 \rightarrow AuAl_2+Pt_2Al_3 \rightarrow AuAl\ (?)+Pt_2Al_3$

after which oxidation occurs, possibly as:

$4AuAl+Pt_2Al_3+3O_2 \rightarrow Au_4Al+2PtAl+2Al_2O_3$

Multi-layer samples

More complex structures could be created by increasing the number of layers deposited. Samples with four, six and eight alternating layers of Al and alternating precious metals were investigated. After annealing at 400° C for 1 hour, the four-layer films reacted to become two separate layers of $PtAl_2$ and $AuAl_2$. The color of the uppermost layer, as determined from the

reflectance spectrum, indicated that the uppermost layer was either pure $PtAl_2$ or pure $AuAl_2$, depending on sequence deposited. Similarly, when multilayer thin films of six and eight layers were deposited and then annealed, it was observed by cross-section analysis that they had reacted to three and four layers respectively. Cross-sections of various permutations of films are shown in Fig. 6. It was evident that, if initially formed separately, then $AuAl_2$ and $PtAl_2$ would not interdiffuse, even after a protracted anneal at 400 °C. Clearly, these phases are immiscible under equilibrium conditions.

Formation of the intermetallic compounds during post-deposition annealing could be followed by *in situ* XRD in a synchrotron. In Fig. 7 the average of the area of the (111), (002), (022) and (113) peaks of $PtAl_2$ and $AuAl_2$ are shown for four layer samples heated at an overall average rate of 3 K/minute but with dwell times of 1 minute in 50 °C steps. Under these conditions, crystallization of the intermetallic phase started at ~180 °C and was substantially complete at ~580 °C. Further heating then reduced the proportion of these phases, possibly due to oxidation or reaction of the thin film with its substrate, or by the decomposition of the C1 phases into other intermetallic compounds.

3.3 Bulk samples produced by arc melting

SEM backscatter and EDS analysis of the bulk $(Au_{0.5}Pt_{0.5})Al_2$, $(Au_{0.7}Pt_{0.3})Al_2$ and $(Au_{0.9}Pt_{0.1})Al_2$ samples showed that the microstructures contained a matrix phase or phases of MAl_2 with close to the nominal sample composition, and a few volume percent of Al-rich interdendritic phase. Due to the similarity of atomic number of Pt and Au, backscatter imaging would not be expected to show up any duplex microstructure of $AuAl_2$ and $PtAl_2$. However, all SEM point analyses of the matrix were similar, indicating that what was being analyzed was $(Au,Pt)Al_2$ solid solution rather than a duplex mixture of $AuAl_2$ and $PtAl_2$. In addition, X-ray diffraction of the $(Au_{0.5}Pt_{0.5})Al_2$ sample revealed well-formed peaks mid-way between those of pure $AuAl_2$ and pure

$PtAl_2$. This is further evidence that a solid solution of the two compounds had formed.

3.4 Optical properties of $AuAl_2$-$PtAl_2$ mixtures and alloys

The reflectance of the $AuAl_2$ and $PtAl_2$ films formed from multi-layer stacks of the elements was compared to that produced by the co-deposition technique, and to data derived from bulk samples (Fig. 8). The CIE La*b* coordinates are compared in Table 1. It should be noted that L*a*b* coordinates are effected by both intrinsic (band structure, presence of second phases) and extrinsic (surface roughness, light source, presence of second phase) factors and the latter, in particular, can be the source of variations between samples. (For example, increased surface roughness reduces the L* parameter and perturbs the a* and b* values in unpredictable ways.) The effective dielectric functions of the colored films of $AuAl_2$ and $PtAl_2$ are shown in Figs. 9(a) and 9(b). The form of the dielectric functions of $PtAl_2$ and $AuAl_2$ is similar. Furthermore, the region in which ε_1 is in the range for localized plasmon resonances ($-1<\varepsilon_1<-10$) is not much effected by the method of sample preparation. However, at higher energies, ε_1 for the thin films crosses zero and become positive. This may be due to one of the extrinsic factors mentioned earlier. The ε_1 reaches its maximum positive value in the thin films at ~ 3.25 eV in $PtAl_2$ and ~2.75 eV in $AuAl_2$.

In the case of the Al/(Au,Pt) sample the effect of front-surface roughness was avoided by optically characterizing the back-surface (taking into account the optical properties of the glass slide). The back surface reflection minimum of this sample was ~440 nm which may be compared to that of pure $PtAl_2$ which is at about ~390 nm and pure $AuAl_2$, which is at ~530 nm. The observed minimum of the alloyed sample is in agreement with the 440 nm estimated from the simple rule of mixtures and the CIE L*a*b* color coordinates are intermediate between those of the pure compounds, Table 1.

4. Discussion

The results described above highlight two interesting issues, which we will discuss in turn.

4.1 How stable is the (Au,Pt)Al_2 solid solution?

There are many examples of mixtures of phases that do not form a mutual solid solution under equilibrium conditions, but which can, nevertheless, be prepared as a metastable solid solution under some circumstances. For example, under equilibrium conditions at temperatures below 1260 °C Au and Pt are immiscible but metastable solid solutions in this system (and related systems such as Au-Ni [22] or W-Ni [23] may be prepared by quenching alloy samples from temperatures above the miscibility gap or by magnetron co-deposition at room temperature. This situation evidently also applies to $AuAl_2$-$PtAl_2$. However, if the two compounds are formed separately, they do not interdiffuse, indicating that the equilibrium situation is one of mutual immiscibility, as suggested by Klotz [5]. The present work has also served to highlight that quite precise control of the deposition and heat-treatment parameters are required to produce the desired phases, in terms of film composition well as time and temperature of the post-temperature heat-treatment.

4.2 What is the possible color gamut that can be achieved using these materials?

As we have seen, it is certainly possible to produce metastable solid solutions of $AuAl_2$-$PtAl_2$ with a corresponding range of intermediate colors. However, it should also be recognized that very similar colors can also be presented to an external observer by fine-scale dual-phase mixtures of $AuAl_2$ and $PtAl_2$. In this respect, the situation in this ternary system is analogous to that in the binary Au-Ni system, where a range of equivalent color effects can be achieved by true alloying or by a two-phase mixture of the elements[22]. We have also provided evidence here to suggest that a (Au,Pt)Al_2 solid solution is metastable, and hence prone to decomposition. In contrast, pure $AuAl_2$

and pure $PtAl_2$ are both stable to relatively high temperatures and, under equilibrium conditions, apparently immiscible. Therefore, it seems that a range of interesting color effects could be engineered by designing thin film stacks of these two intermetallic compounds. Such a scheme could be easier to control than one requiring the fabrication of a metastable film of $(Au,Pt)Al_2$.

To investigate this, optical properties of a wide range of possible bi-layer film designs were simulated with the OpenFilter program. The calculated reflectance spectra (calculated using the dielectric functions of the pure $AuAl_2$ or $PtAl_2$ thin films) are shown in Fig. 10.The color is shifted between yellow and purple when the thickness of top layer is varied from 0 to 100 nm. CIE *L*a*b** color parameters of these bi-layer films were predicted and shown in Table 2. Unsurprisingly, the calculated colors of the two series ($AuAl_2$-on-$PtAl_2$ and $PtAl_2$-on-$AuAl_2$) follow quite different trajectories through color space, Fig. 11. In particular, the prediction is that the colors obtained by depositing $AuAl_2$ onto $PtAl_2$ are much more saturated than vice versa. This comes about due to the differences in the optical properties in the visible region of the two materials. As the two metals absorb at different wavelength ranges, ~ 400 and ~540 nm, each is either a mirror or absorber at 400 and 540 nm, while the other in the complementary mode. This interplay of absorptive and reflective factors produces an interesting range of colors. Similar effects have recently been discussed by Kats et al. [24], in this case for nanoscale coatings of Ge on Au.

Several measurements of the L*a*b* coordinates of pure $AuAl_2$ and $PtAl_2$ samples from our work or from the literature are also shown in Fig. 11. There is a scatter of the values due to the intrinsic and extrinsic factors mentioned previously. Also shown on Fig.11 are the color coordinates of our bulk samples and those of the thin film samples of Furrer and Spolenak [8]. It is clear that the measured colors of the $(Au,Pt)Al_2$ are broadly similar (although slightly more intense) than the colors we predict for thin films of $AuAl_2$ on $PtAl_2$.

5. Conclusion

The color gamut of thin films comprised of mixtures of $AuAl_2$ and $PtAl_2$ can be tuned by control of their geometry, microstructure and composition. We conclude that a very similar range of colors can be obtained if two compounds are in separate layers of nanoscale thickness, or in the form of a nanoscale coating on $AuAl_2$ on bulk $PtAl_2$, or in a random duplex microstructure, or in a metastable solid solution. These findings provide several strategies to smoothly vary the reflected spectrum of a coated object from the metallic purple hue of $AuAl_2$ to the gold-yellow hue of $PtAl_2$. Colors in-between can be described as lavender, apricot or peach. There is apparently no ternary phase diagram available yet for the Al-Au-Pt ternary system, but the work presented here indicates that, under equilibrium conditions, $AuAl_2$ and $PtAl_2$ are likely to be distinct and mutually insoluble phases. Nevertheless, metastable solid solutions of the $(Au,Pt)Al_2$ type can be prepared by co-deposition or rapid solidification. The precious metal content of the films remains above 76 weight % suggesting that they might find application in jewelry as an alternative to using the more expensive and brittle bulk compounds.

Acknowledgement

S.S. acknowledges the support of a Royal Thai Scholarship. Part of this research was undertaken on the Powder Diffraction beamline at the Australian Synchrotron, Victoria, Australia and we thank beamline scientists Dr Quinfen Gu and Dr Justin Kimpton for assistance. The Advanced Materials Division of Mintek, South Africa manufactured the bulk samples.

References

[1] S.G. Steinemann, W. Wolf, R. Podloucky, Color and optical properties, in: J.H. Westbrook, R.L. Fleischer (Eds.) Intermetallic Compounds – Principles and Practice – Volume 3: Progress, John Wiley & Sons Ltd 2002, pp. 231-244S.

[2] R.A. Varin, Intermetallics: Crystal structures, in: J.W. Martin (Ed.) Concise Encyclopedia of the Structure of Materials 2007.

[3] J. Hurly, P.T. Wedepohl, Optical properties of colored platinum intermetallic compounds, J. Mater. Sci., 28 (1993) 5648-5653.

[4] S. Supansomboon, A. Maaroof, M.B. Cortie, "Purple glory": The optical properties and technology of $AuAl_2$ coatings, Gold Bull., 41 (2008) 296-304.

[5] U.E. Klotz, Metallurgy and processing of coloured gold intermetallics – Part I: Properties and surface processing, Gold Bull., 43 (2010) 4-10.

[6] J. Fischer-Bühner, A. Basso, M. Poliero, Metallurgy and processing of coloured gold intermetallics - Part II: Investment casting and related alloy design, Gold Bull., 43 (2010) 11-20.

[7] E. van der Lingen, Aspects of coloured precious metal intermetallic compounds, J. of the S. Afr. Inst. Mining Metall., 114 (2014) 137-144.

[8] A. Furrer, R. Spolenak, Colors of thin films of binary and ternary gold- and platinum-based alloys, Acta Mater., 66 (2014) 241–250.

[9] V.J. Keast, K. Birt, C.T. Koch, S. Supansomboon, M.B. Cortie, The role of plasmons and interband transitions in the color of $AuAl_2$, $AuIn_2$ and $AuGa_2$, App. Phys. Lett., 99 (2011) 111908.

[10] V.J. Keast, B. Zwan, S. Supansomboon, M.B. Cortie, P.O.Å. Persson, $AuAl_2$ and $PtAl_2$ as potential plasmonic materials, J. Alloys Compd., 577 (2013) 581-586.

[11] M.G. Blaber, M.D. Arnold, M.J. Ford, A review of the optical properties of alloys and intermetallics for plasmonics, J. Phys.: Condens. Matter 22 (2010) 143201.

[12] L. Chen, D. Lynch, The optical properties of $AuAl_2$ and $PtAl_2$, phys. stat. sol. (b), 148 (1988) 387-394.

[13] A. Gupta, R.S. Gupta, Electronic and optical properties of $AuAl_2$ and $PtAl_2$, phys. stat. sol. (b),

168 (1991) 455-465.

[14] H.R. Philipp, $AuAl_2$: Optical properties and consideration as a transparent electrode material, phys. stat. sol. (a), 69 (1982) 547-551.

[15] S.S. Vishnubhatla, J.P. Jan, Optical properties of the intermetallic compounds $AuAl_2$, $AuGa_2$ and $AuIn_2$, Philos. Mag., 16 (1967) 45-50.

[16] S. Miyama, Purple sintered gold alloy for ornamentation, Jap. Pat. 19860083026, 1987.

[17] S. Yamasaki, N. Ishii, K. Sawada, Noble metal ornament member and its production method, and ornament part and accessory part, Jap. Pat., 2003183710A, 2003.

[18] C. Cretu, E. van der Lingen, Coloured gold alloys, Gold Bull., 32 (1999) 115-126.

[19] S. Larouche, L. Martinu, OpenFilters: open-source software for the design, optimization, and synthesis of optical filters, Appl. Opt., 47 (2008) C219-C230.

[20] E308-01, Standard Practice for Computing the Colors of Objects by Using the CIE System, American Society for Testing and Materials (ASTM), 2001.

[21] P. Villars, Pearson's Handbook of Crystallographic Data for Intermetallic Phases, ASM International, Materilals Park, Ohio, 1991.

[22] D.J. McPherson, S. Supansomboon, B. Zwan, V.J. Keast, D.L. Cortie, A. Gentle, A. Dowd, M.B. Cortie, Strategies to control the spectral properties of Au-Ni thin films, Thin Sol. Films, 551 (2014) 200-204.

[23] C. Borgia, T. Scharowsky, A. Furrer, C. Solenthaler, R. Spolenak, A combinatorial study on the influence of elemental composition and heat treatment on the phase composition, microstructure and mechanical properties of Ni-W alloy thin films, Acta Mater., 59 (2011) 386-399.

[24] M.A. Kats, R. Blanchard, P. Genevet, F. Capasso, Nanometre optical coatings based on strong interference effects in highly absorbing media, Nat. Mater., 12 (2013) 20-24.

Tables

Table 1. CIE L*a*b* color coordinates of experimental films and bulk samples

	L*	a*	b*
$PtAl_2$ (co-deposit)	78.05	0.33	14.96
$PtAl_2$ (stack)	79.5	1.20	23.66
$PtAl_2$ (bulk)	76.30	2.14	12.97
$AuAl_2$ (co-deposit)	68.39	17.79	-4.42
$AuAl_2$ (stack)	65.2	23.38	-9.20
$AuAl_2$ (bulk)	70.18	10.00	-6.02

Table 2. Predicted CIE L*a*b* color parameters of a nanoscale layer of one aluminide on the other. (a) 200 nm $PtAl_2$ film that has been over-coated with indicated thickness of $AuAl_2$ (b) 200 nm $AuAl_2$ that has been overcoated with indicated thickness of $PtAl_2$.

(a)

Thickness of $AuAl_2$ (nm)	L*	a*	b*
0	78.714	3.243	23.199
5	73.579	12.149	23.283
10	69.248	21.699	13.927
20	64.435	33.441	-3.293
40	63.431	26.449	-14.766
100	65.590	18.694	-9.244

(b)

Thickness of $PtAl_2$ (nm)	L*	a*	b*
0	65.474	19.154	-9.523
5	69.315	15.140	-5.222
10	72.250	11.783	-1.231
20	76.057	6.768	6.284
40	78.817	2.189	18.053
100	78.775	3.036	23.548

Figures

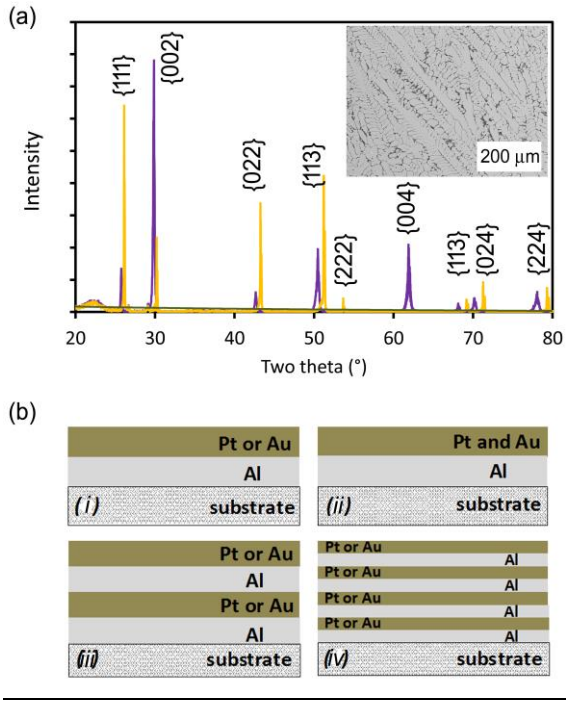

Fig. 1. (a) X-ray diffraction patterns of vacuum arc cast samples of $AuAl_2$ and $PtAl_2$ showing C1 crystal structure. Inset. Microstructure of cast $AuAl_2$ samples showing dendritic solidification. (b) Design of multi-layered stacks for the synthesis of thin films of $AuAl_2$, $PtAl_2$ and $(Au,Pt)Al_2$.

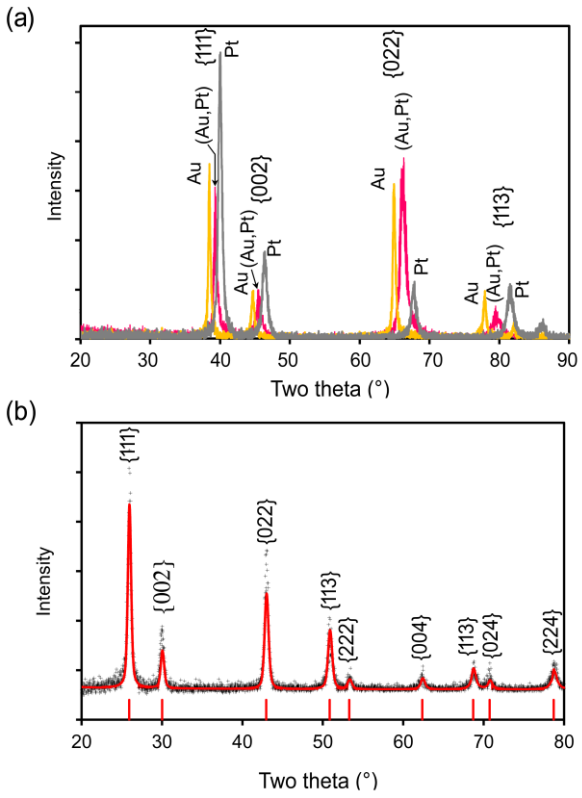

Fig. 2. X-ray diffraction of multilayers. (a) A comparison of X-ray patterns of thin films of (Au,Pt) solid solution to those of pure Au and pure Pt.(b) X-ray pattern of sample of Al/(Au,Pt) formed by co-depositing Au and Pt onto Al. Fitted profile obtained by Rietveld refinement on an anti-fluorite C1 structure with lattice parameter intermediate between $AuAl_2$ and $PtAl_2$.

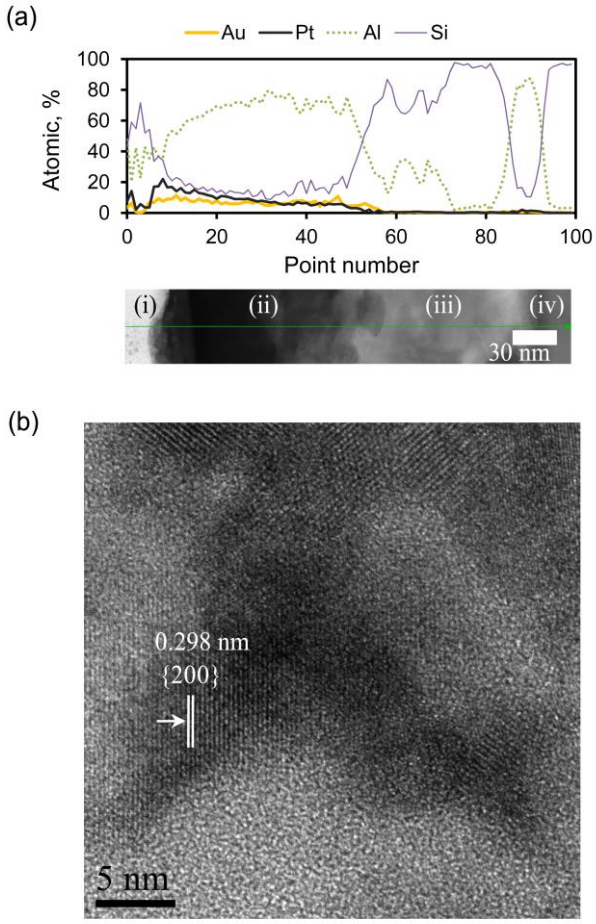

Fig. 3. Microstructure of multilayers. (a) TEM EDS elemental scan through thin film of Al/(Au,Pt) from top surface on left to silicon substrate on right, (i) mounting resin, (ii) $(Au,Pt)Al_2$ layer, (iii) Al + Si layers, and (iv) silicon substrate. Sample has been annealed at 400 °C for 2 h. (b) High resolution TEM image of 20 nm Au+Pt on Al film, after heat treatment. Prominent fringes have a ~0.30 nm spacing and correspond to the {002} *d*-spacing of $(Au,Pt)Al_2$.

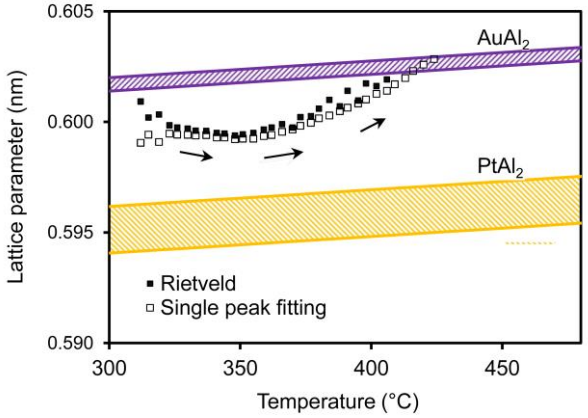

Fig. 4. Lattice parameter of C1 phase in the Al/(Au,Pt) sample as a function of temperature as sample is heated. Estimates obtained from Rietveld full pattern refinement and from fitting a pseudoVoight to the {111} peak are shown. Also shown are scatter bands for the estimated lattice parameters of pure $AuAl_2$ and $PtAl_2$ as a function of temperature. The X-ray diffraction patterns of the bulk $AuAl_2$ and bulk $PtAl_2$ phases at room temperature are shown as insets.

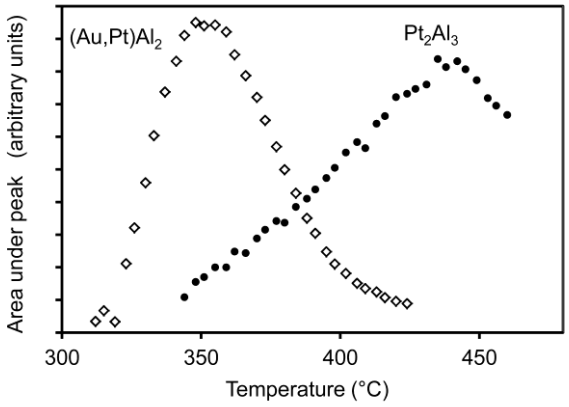

Fig. 5. Peak area of the {111} of the $(Au,Pt)Al_2$ phase and {002} of the Pt_2Al_3 phase in Al/(Au,Pt) sample as a function of temperature during heating.

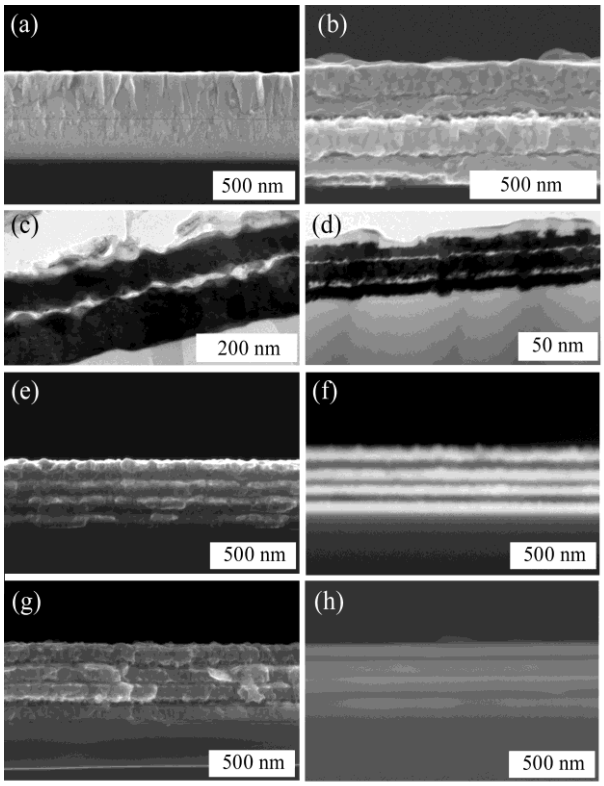

Fig. 6 (a) Cross-sectional TEM and SEM views of two, four and six-layered films.(a) Cross-sectional SEM view of two-layer sample produced by co-depositing Al and Pt, then Al and Au. Sample then annealed at 400 °C for 24 h. EDS indicates no interdiffusion of the $PtAl_2$ and $AuAl_2$. (b) Cross-sectional SEM view of eight-layer sample of elements (Al-Pt-Al-Au-Al-Pt-Al-Au) after annealing at 400 °C for 0.5 h. From bottom to top, sample consists on alternating layers of $PtAl_2$-$AuAl_2$-$PtAl_2$-$AuAl_2$. (c) Cross-sectional TEM view of four-layered film of Al/Au/Al/Pt on Si substrate after annealing, (d) cross-sectional TEM view of six-layered sample after annealing, (e) 'in-lens' mode SEM cross- section of eight-layered films of Al-Au-Pt before annealing at 400 °C (f) backscatter image of same sample as (e), (g) 'in lens' SEM image of eight-layered sample after annealing at 400 °C, (h) backscatter SEM image of same sample as (g).

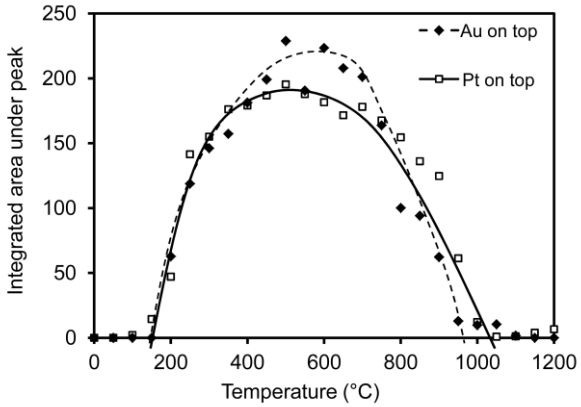

Fig. 7. Average of the integrated peak areas of $PtAl_2$ and/or $AuAl_2$ over the {111}, {200}, {220} and {311} peaks as a function of temperature. The two samples were produced as Al+Pt+Al+Au ('Au on top') and Al+Au+Al+Pt ('Pt on top'). Substrate was tantalum foil.

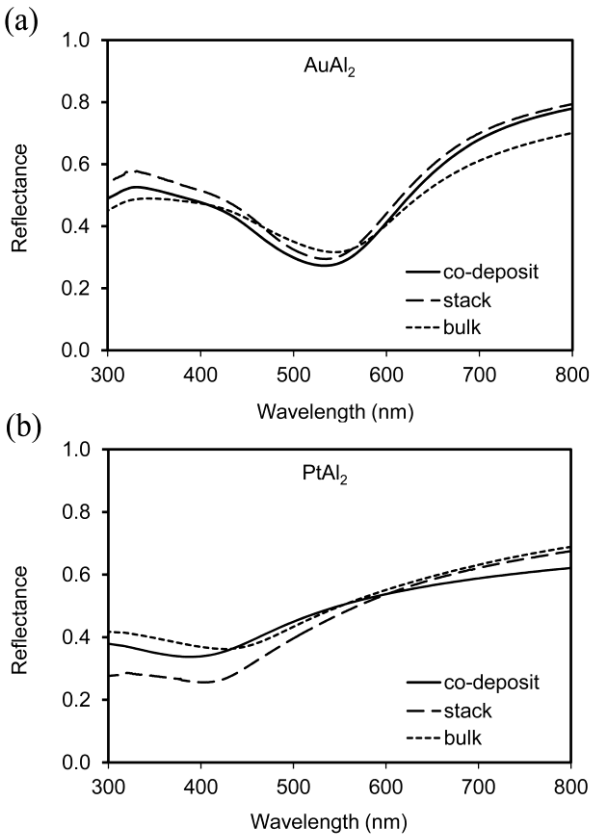

Fig. 8. Reflectance spectra of $AuAl_2$ and $PtAl_2$ produced by co-deposition with annealing, deposition of elemental stacks followed by annealing, and bulk material produced by vacuum arc

melting, (a) $AuAl_2$ produced by having Au as the top layer, (b) $PtAl_2$ produced with Pt as top layer.

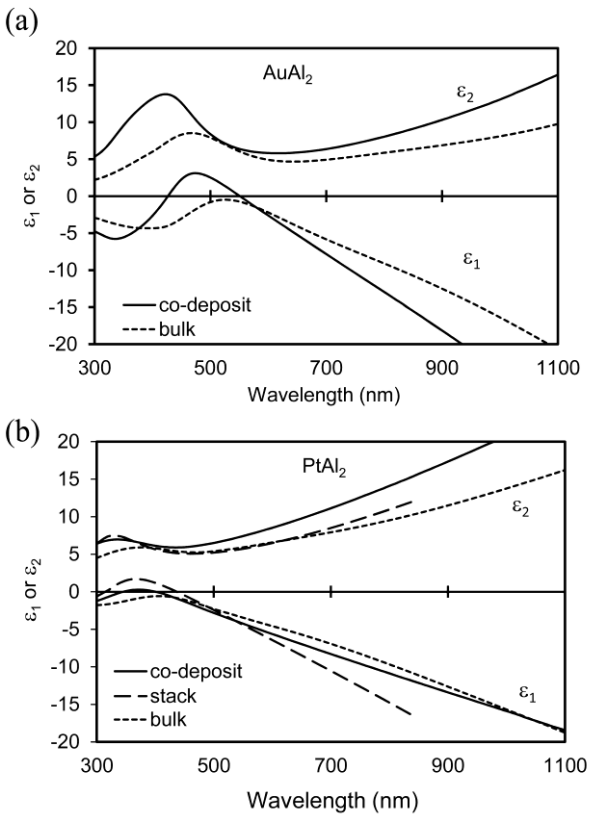

Fig. 9. Dielectric constants of colored intermetallic compounds produced by co-deposition of the binary mixture Au+Al or Pt+Al, followed by annealing, compared to that of bulk material produced by vacuum arc melting, (a) $AuAl_2$, (b) $PtAl_2$. The dielectric function of a $PtAl_2$ formed from a stack of the elements is also shown.

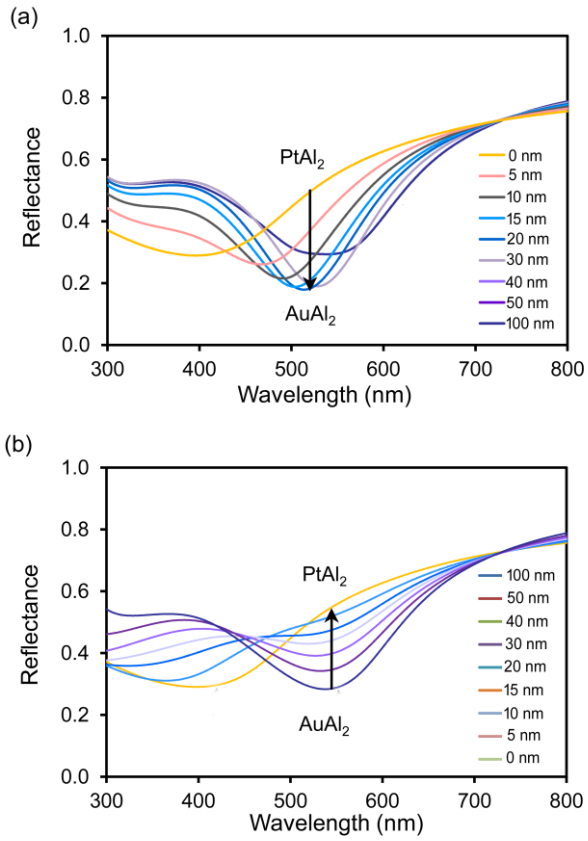

Fig. 10. Calculated reflectance of bi-layers of $PtAl_2$ and $AuAl_2$. Calculations made using dielectric function of co-deposited samples. The direction of increase in thickness of the top layer is indicated by an arrow. (a) 200 nm $PtAl_2$ film that has been over-coated with indicated thickness of $AuAl_2$ and (b) 200 nm $AuAl_2$ film that has been over-coated with indicated thickness of $PtAl_2$.

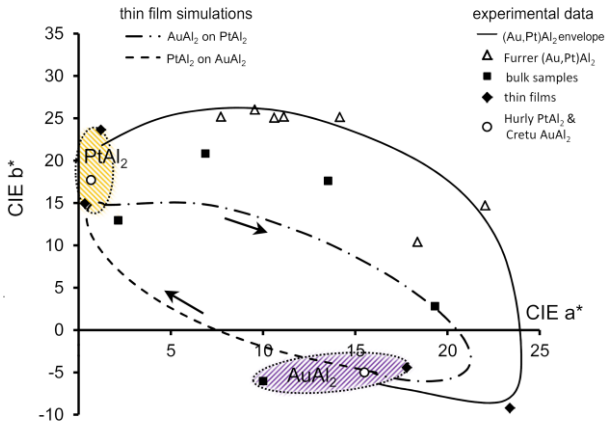

Fig.11. Color gamut of $AuAl_2$ / $PtAl_2$ microstructures plotted in CIE L*a*b* space. The predicted

color gamuts of the thin film stacks obtained by depositing $AuAl_2$ on $PtAl_2$, and vice versa, are shown. The colors of the bulk samples and literature data (Hurly [3] and Cretu[18]) are also shown for comparison. (The color coordinates of the thin film samples of Furrer & Spolenak [8] were obtained by digitizing their published reflectance data.)